scientific reports

Check for updates

OPEN

Biogenic synthesis of gold nanoparticles using *Coleus forskohlii* leaf extract enhances anticancer activity against HT-29 cells and modulates the p53 regulated immune microenvironment in colon adenocarcinoma

Muath Suliman[1], Essam H. Ibrahim[2,3]✉, Mohammad Y. Alshahrani[1], Mona Kilany[4], Rabah N. Alsulami[5], Zenat Khired[6], Hussam M. Shubaily[7], Attalla F. El-kott[2,8], Ahmed Ezzat Ahmed[2] & Salama A. Salama[9]

Colorectal cancer remains a leading cause of cancer-related mortality worldwide, underscoring the urgent need for novel therapeutic strategies. In this study, we hypothesized that the synergistic combination of *Coleus forskohlii* leaf extract (CFLE) and its biogenically synthesized nanogold would enhance anticancer efficacy against HT-29 human colon adenocarcinoma cells by modulating reactive oxygen species (ROS) production and activating the tumor suppressor protein p53. Aqueous CFLE was prepared from dried leaves and used to synthesize gold nanoparticles, which were characterized by UV-Vis spectrophotometry, X-ray diffraction (XRD), and Fourier-transform infrared (FT-IR) spectroscopy. FT-IR analysis confirmed the presence of bioactive phytochemicals in CFLE capable of reducing and stabilizing the nanogold. Both CFLE and CFLE + nanogold demonstrated dose-dependent inhibition of HT-29 cell viability, accompanied by elevated ROS levels and significant upregulation of p53 expression. Combining of CFLE with the nanogold (extract + nanogold) could cancel the toxic effects of gold nanoparticles. Complementary bioinformatic analyses of colon adenocarcinoma datasets revealed that high *TP53* expression correlates with improved patient survival and enhanced immune infiltration, particularly of B plasma cells, neutrophils, and M2 macrophages, mediated through chemokine signaling pathways. Our findings highlight the dual anticancer and antimicrobial potential of CFLE and CFLE + nanogold, with the nanocomposite formulation offering a novel, plant-based approach to colon cancer therapy through ROS-mediated p53 activation. In addition, CFLE could pause the toxic effects of the gold nanoparticles. This work positions *TP53* not only as a central mechanistic node in CFLE + nanogold-induced cytotoxicity but also as a robust prognostic biomarker in colorectal cancer.

Keywords HT-29, p53 protein, Colon adenocarcinoma, Nanogold, Immune microenvironment

[1]Department of Clinical Laboratory Sciences, College of Applied Medical Sciences, King Khalid University, P.O. Box 61413, Abha 9088, Saudi Arabia. [2]Department of Biology, College of Science, King Khalid University, P.O. Box 61413, Abha 9088, Saudi Arabia. [3]Blood Products Quality Control and Research Department, National Organization for Research and Control of Biologicals, Cairo, Egypt. [4]Department of Microbiology, National Organization for Drug Control and Research (NODCAR), Cairo, Egypt. [5]Department of Biology, College of Applied Sciences, Umm Al-Qura University, Mecca, Saudi Arabia. [6]Surgical Department, Faculty of Medicine, Jazan University, Jazan, Saudi Arabia. [7]Department of Basic Medical Sciences (Pathology), Jazan University, Jazan, Saudi Arabia. [8]Department of Zoology, Faculty of Science, Damanhour University, Damanhour, Egypt. [9]Department of Biology, College of Science, Jazan University, P.O. Box 114, Jazan 45142, Saudi Arabia. ✉email: essamebrahim@hotmail.com

Colorectal cancer is the third most common cancer worldwide. It has been shown to occur at particularly high rates in Europe, North America, Australia, and New Zealand, while historically lower incidence rates have been reported in Asia, Central and South America, and Africa. However, the incidence of colorectal cancer is rising steadily in these latter regions[1]. Epidemiological studies have shown that regular consumption of fruits and vegetables may reduce the risk of epithelial carcinomas such as cancers of the colon, pharynx, esophagus, lung, stomach, larynx, and cervix. Data from the European Prospective Investigation into Cancer and Nutrition (EPIC) suggest that daily intake of 450–500 g of vegetables and fruits can lower the incidence of various digestive tract cancers by up to 25%[2,3].

Plants have long served as a vital source of therapeutic agents and remain a cornerstone in the discovery of new drugs particularly for cancer and other diseases that currently lack effective cures. Today, a vast array of medicinal plant species contributes significantly to the development of modern pharmaceuticals. Natural compounds derived from these plants hold immense promise for the discovery and development of novel therapeutics targeting a wide spectrum of human diseases[4]. *Coleus forskohlii* is a member of the Lamiaceae family. Commonly known as Coleus in English, this species is widely distributed across several countries, including Nepal, Thailand, India, and regions of the Mediterranean[5]. Many studies showed that the perennial plant *C. forskohlii* contains reducing sugars, terpenoids, tannins, flavonoids, and alkaloids[6]. Flavonoids, a class of polyphenolic compounds, are widely recognized for their health-promoting properties, including anti-inflammatory, antioxidant, antimicrobial, anticancer, and anti-allergic activities[7,8]. *Coleus forskohlii* can be used to treat many disorders like problems in the heart, respiratory problems, colic, convulsion, asthma, insomnia, burning sensation, intestinal disorder, constipation, inflammatory diseases, hypertension, aging, epilepsy, weight management and angina[9–11]. It has been demonstrated that natural bioactive compounds, such as saponins, phenolics, alkaloids, tannins, and terpenoids, can exert beneficial health effects by scavenging free radicals[12].

It was reported that forskolin is the major active biomolecule in *Coleus forskohlii* root. Forskolin is a labdane diterpene that has a weight-loss property. *Coleus forskohlii* is known to have a large amount of forskolin among plants[10]. The mechanism of Forskolin action is the increase of cyclic adenosine monophosphate (cAMP) accumulation avoiding adenylate cyclase hormonal stimulation[10,13], a step leading to activation of lipases followed by lipolysis, so forskolin acts as an anti-obesity molecule[13–15].

Green metal nanotechnology plays a pivotal role in developing innovative and improved therapeutic strategies for various diseases. Biological synthesis of metal nanoparticles, particularly using plant extracts, has emerged as a superior alternative to conventional chemical methods. This approach is favored for its high biocompatibility, eco-friendly nature, and non-toxic profile, which collectively enhance its suitability for biomedical applications and biological synergy[16].

Despite the promising anticancer potential of AuNPs, several critical challenges limit their clinical application in colon cancer treatment. First, conventionally synthesized AuNPs often rely on toxic chemical reductants and stabilizers, raising concerns about biocompatibility and long-term safety. Second, many AuNP formulations lack tumor selectivity, leading to off-target effects and reduced therapeutic efficacy. Third, the mechanisms underlying AuNP-induced cytotoxicity in colorectal cancer, particularly their interactions with key tumor suppressor pathways such as p53 and redox signaling, are not fully elucidated. Moreover, most studies focus solely on nanoparticle delivery or photothermal effects, with limited integration of intrinsic bioactive properties from natural sources that could synergistically enhance anticancer activity. Finally, there is a scarcity of research combining green-synthesized AuNPs with comprehensive bioinformatic validation of molecular targets and immune-modulatory effects in colon adenocarcinoma.

These gaps underscore the need for safer, more targeted, and mechanistically informed nanotherapeutics, such as biogenic nanogold derived from *Coleus forskohlii*, that harness both the physicochemical advantages of nanoparticles and the therapeutic phytochemistry of medicinal plants.

In the present study, the biological properties of *Coleus forskohlii* leaf extract (CFLE) and its biogenically synthesized gold nanoparticles were investigated in HT-29 colon cancer cells. The extract's capacity to synthesize gold nanoparticles and its antimicrobial activity were also evaluated.

Results

Nanogold production

The change in $AuCl_4$/CFLE mixture (Fig. 1A and C) color was an indication of Nanogold production. This change was inspected spectrophotometrically and observed through the color alteration of the mixture (Fig. 1B and D). Figure 1D indicates that the peak absorbance is at 520 nm which is specific to gold nanoparticles.

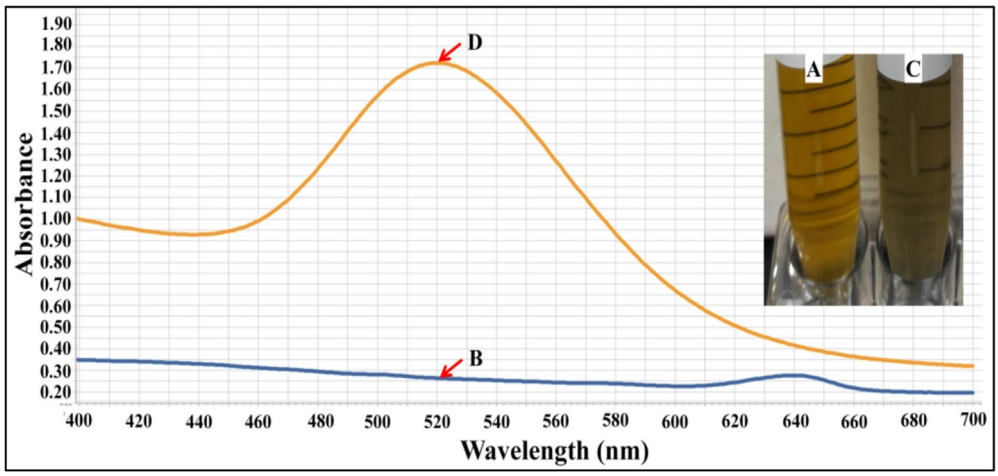

Fig. 1. UV-Visible absorption spectra illustrating the biosynthesis of gold nanoparticles using *Coleus forskohlii* leaf extract (CFLE). Where A: visual appearance/color of the plant extract alone; Curve B: absorbance spectrum of *C. forskohlii* leaf extract (baseline control), showing broad absorption in the UV region (400–700 nm) due to phytochemicals; **C**: visual appearance/color of the reaction mixture after addition of $HAuCl_4$ and incubation (typically turns ruby red/purple, indicating nanoparticle formation); Curve D: UV-Vis spectrum of the *C. forskohlii* extract after AuNP synthesis, exhibiting a distinct surface plasmon resonance (SPR) peak centered at about 520 nm, characteristic of spherical gold nanoparticles.

X-ray diffraction

Figure 2 demonstrates the patterns of X-ray diffraction (XRD) of nanogold manufactured by CFLE. The pattern matches JCPDS (Joint Committee on Powder Diffraction Standards) file No. 04-0784, which corresponds to pure metallic gold (Au^0) with a face-centered cubic (fcc) crystal structure[17]. The relative intensity order—with the (111) plane being the strongest—is typical for spherical or quasi-spherical gold nanoparticles and reflects their thermodynamically stable surface orientation.

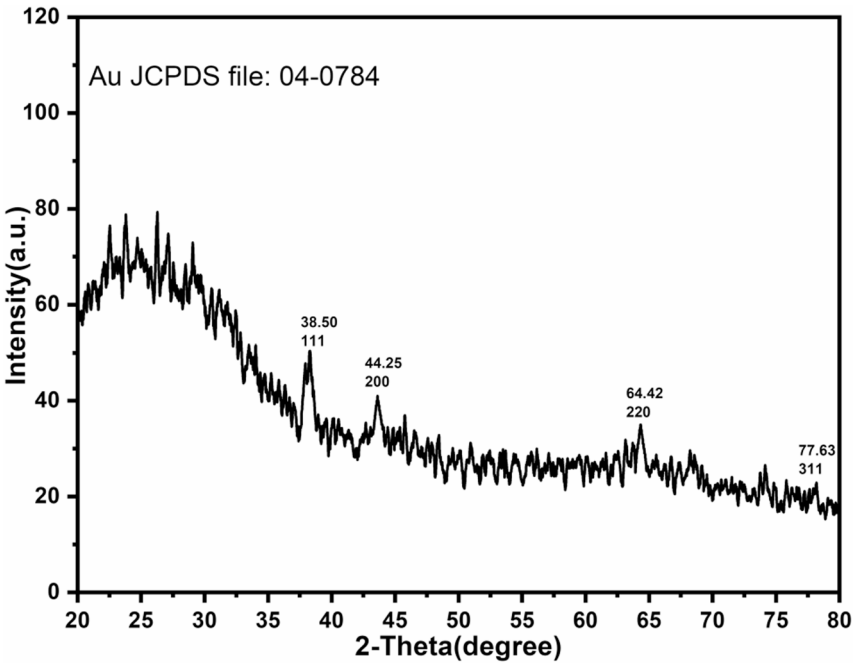

Fig. 2. X-ray diffraction pattern of biologically synthesized gold nanoparticles using *Coleus forskohlii* leaf extract as a green reducing and stabilizing agent. The diffractogram shows distinct Bragg reflection peaks at $2\theta \approx 38.50°$, 44.25°, 64.42°, and 77.63°, corresponding to the (111), (200), (220), and (311) crystallographic planes of face-centered cubic (fcc) metallic gold (JCPDS card no. 04-0784). The sharp, well-defined peaks confirm the crystalline nature and phase purity of the biosynthesized nanogold.

2theta	HKL	FHWM	Grain size	Assignment
38.50	111	0.228	36.89	Most intense peak; dominant facet in fcc gold nanoparticles
43.61	200	0.167	51.39	Secondary intense reflection
64.42	220	0.108	86.63	Higher-order reflection
77.63	311	0.168	60.70	Confirms fcc lattice symmetry
Average crystallite size			58.90	

Table 1. X-ray diffraction peak parameters of biosynthesized Nanogold using *Coleus forskohlii* leaf extract (CFLE) as a green reducing and capping agent.

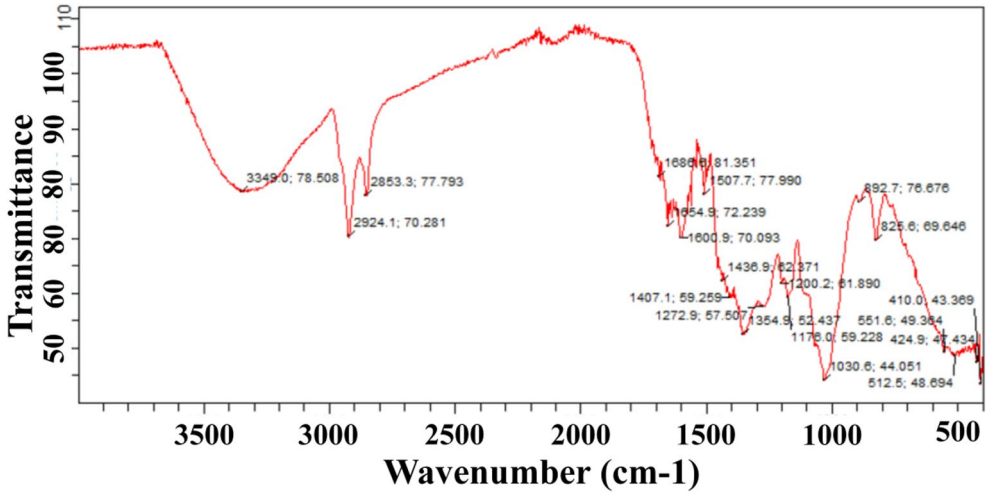

Fig. 3. Fourier-transform infrared (FTIR) absorption spectrum of a crude water extract from *Coleus forskohlii* leaves, recorded in the mid-infrared region (400–3500 cm^{-1}).

Table 1 shows peaks at 2θ of 38.50o, 44.65o, 64.42o and 77.63 might be a result of the crystallographic planes 111, 200, 220 and 311. The other observed peaks may be due to the bio-organic phase crystallization occurring on the surface of the nanogold[18]. The average crystalline size was estimated to be 58.29 nm.

Functional groups

Fourier transform infrared (FTIR, Fig. 3) is quite a popular analytical technique for characterizing chemical compounds. The spectrum highlights characteristic vibrational bands corresponding to functional groups present in bioactive phytochemicals, including alcohols, alkenes, carbonyls, and aromatic systems. Key absorption peaks are labeled with their wavenumbers (cm^{-1}) and approximate transmittance (%) values, revealing the molecular complexity and chemical diversity of the extract. Fourier-transform infrared spectroscopy identified the bioactive phytoconstituents in *Coleus forskohlii* leaf extract (CFLE) responsible for the bio-reduction and capping of gold nanoparticles (AuNPs). The FTIR spectrum of CFLE exhibited characteristic absorption bands at 3349.0 cm^{-1} (O–H stretching of phenolics and alcohols), 1654.9 cm^{-1} (C = O stretching of carbonyl groups in flavonoids or terpenoids), and 1600.9 cm^{-1} (aromatic C = C stretching), all of which are consistent with known reducing and stabilizing agents in plant-mediated nanoparticle synthesis.

Extract cytotoxicity against HT-29 cancer cell line

The crude leaf extract showed no cytotoxic effect, with cell viability consistently near or above 100% across all concentrations when compared to untreated control cells. In stark contrast, the nano-formulated extract (CFLE + nanogold) demonstrated potent, dose-dependent cytotoxicity, reducing cell viability significantly ($p > 0.001$) to 15.14% (84.86% inhibition) at the highest concentration (1000 µg/mL), 84.36% growth at 250 µg/mL (moderate inhibition) and growth approached 100% at ≤ 125 µg/mL. The IC_{50} (half-maximal inhibitory concentration) for CFLE + nanogold lies between 250 µg/mL and 500 µg/mL (Fig. 4).

p53 gene expression

The p53 expression was quantitatively studied after HT-29 cells were treated with the IC_{50} dose of CFLE and CFLE + nanogold in *vitro* using Real-time RT-PCR.

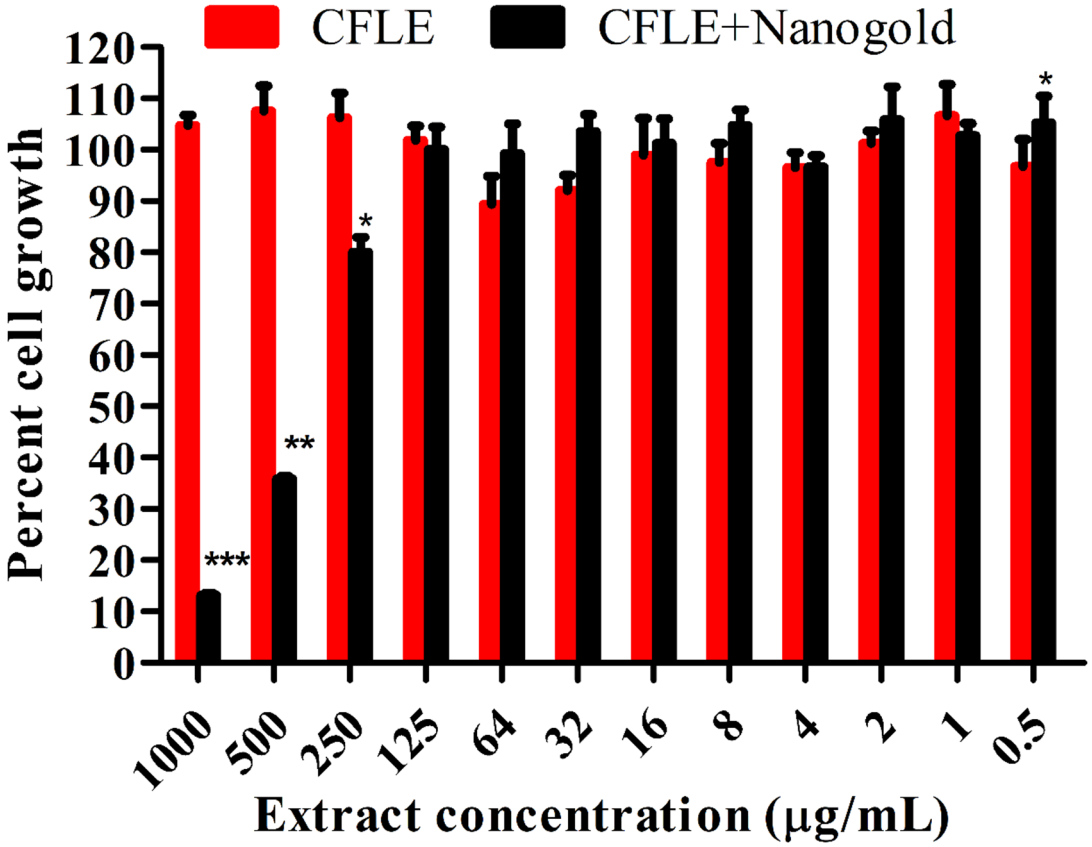

Fig. 4. Percent of HT-29 cell growth stimulation/inhibition after treatment with CFLE and CFLE + nanogold. Data are presented as mean ± standard error ($n = 5$); asterisks indicate statistical significance: * = $P < 0.05$, ** = $P < 0.01$, and *** = $P < 0.001$.

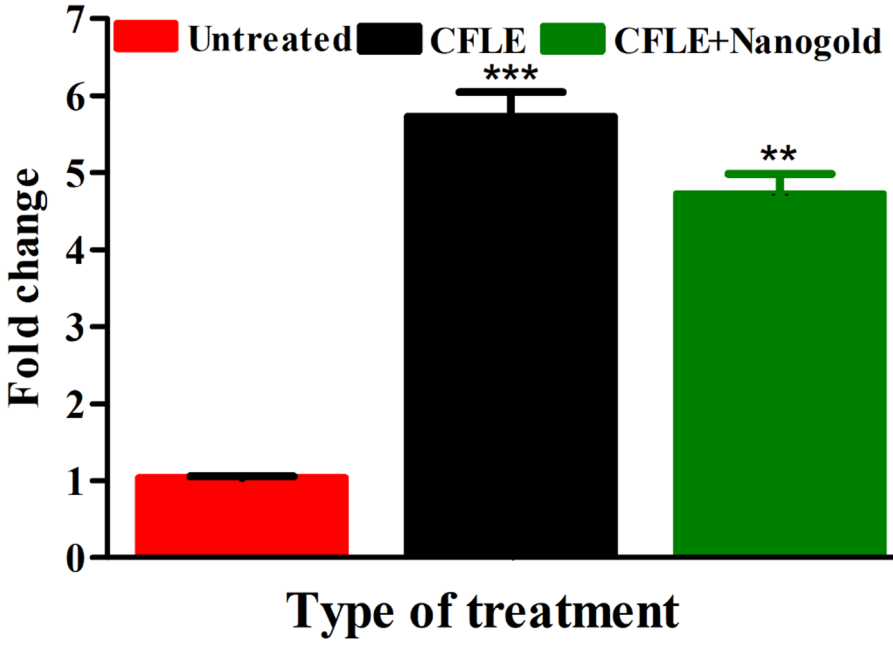

Fig. 5. A p53 gene expression folds increase of HT-29 cells treated with IC_{50} doses CFLE and CFLE + nanogold over untreated cells. Data are presented as mean ± standard error ($n = 5$); asterisks indicate statistical significance: ** = $P < 0.01$, and *** = $P < 0.001$.

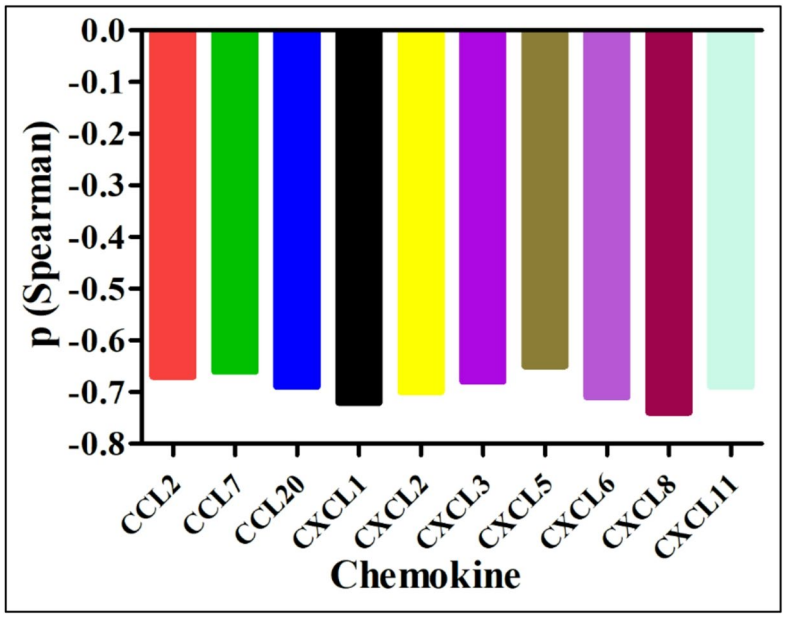

Fig. 6. Substantial negative correlations: TPS3 expression vs. chemokines in COAD (TCGA via TISIDB.

Type of treatment	Inhibition zone (mm)			
	E. coli	*P.* aeruginosa	B. subtilis	Staphylococcus aureus
CFLE	0	7.3 ± 0.18	0	10.50 ± 0.13
CFLE + nanogold	8.20 ± 0.12**	14.10 ± 0.15**	13.70 ± 0.19**	9.80 ± 0.18
Ciprofloxacin (5 µg)	26.23 ± 0.28***	41.75 ± 0.19***	36.92 ± 0.13***	39.60 ± 0.29***

Table 2. Comparative antimicrobial efficacy of CFLE, CFLE-containing biosynthesized gold nanoparticles (CFLE + nanogold), and the standard antibiotic Ciprofloxacin against Gram-negative and Gram-positive bacteria. Data are presented as mean ± standard error ($n = 5$); asterisks indicate statistical significance: ** = $P < 0.01$, and *** = $P < 0.001$.

Results (Fig. 5) exhibited that p53 mRNA expression of HT-29 cells treated with IC_{50} of CFLE significantly ($P < 0.001$) expanded 5.53 folds when compared to control untreated cells while significantly ($P < 0.01$) expanded 4.44 folds when treated with IC_{50} of CFLE + nanogold.

Antimicrobial potential

The antimicrobial efficacy of CFLE, CFLE + nanogold, and ciprofloxacin was assessed by measuring inhibition zones against the tested bacterial strains (Table 2). Against *E. coli*, CFLE showed no inhibitory activity (0 mm), while CFLE + nanogold exhibited a significant inhibition zone of 8.20 ± 0.12 mm ($p < 0.001$ vs. CFLE). Ciprofloxacin produced a substantially larger zone (26.23 ± 0.28 mm; $p < 0.001$ vs. both CFLE and CFLE + nanogold).

Against *P. aeruginosa*, CFLE showed moderate activity (7.30 ± 0.18 mm). The addition of nanogold significantly enhanced inhibition to 14.10 ± 0.15 mm ($p < 0.001$ vs. CFLE). Ciprofloxacin showed the highest activity (41.75 ± 0.19 mm; $p < 0.001$ vs. both plant-based treatments).

Against *B. subtilis*, no activity was observed with CFLE (0 mm), whereas CFLE + nanogold induced a marked inhibition zone of 13.70 ± 0.19 mm ($p < 0.001$). Ciprofloxacin displayed strong inhibition (36.92 ± 0.13 mm; $p < 0.001$ vs. CFLE + nanogold).

Against *S. aureus*, CFLE alone exhibited 10.50 ± 0.13 mm inhibition zone. Interestingly, the CFLE + nanogold combination showed a slightly reduced zone (9.80 ± 0.18 mm), though this difference was not statistically significant ($p = 0.07$). Ciprofloxacin remained highly effective (39.60 ± 0.29 mm; $p < 0.001$ vs. both).

The MIC analysis revealed that CFLE alone exhibited selective antimicrobial activity, being ineffective against *E. coli* and *B. subtilis* (MIC > 1000 µg/mL) but moderately active against *P. aeruginosa* (MIC 500–1000 µg/mL) and *S. aureus* (MIC 250–500 µg/mL). In contrast, CFLE + nanogold showed broad-spectrum enhancement, with MIC values reduced to 125–500 µg/mL across all tested strains. Notably, activity against *P. aeruginosa* and *B. subtilis*, previously weak or absent, was significantly potentiated upon nanogold conjugation. As expected, ciprofloxacin displayed strong activity (MIC < 125 µg/mL) against all bacteria, serving as a positive control.

Survival endpoint	Hazard ratio (HR)	95% confidence interval	*p*-value
Overall survival (OS)	0.61	0.48–0.78	< 0.001
Disease-specific Ssurvival (DSS)	0.59	0.45–0.77	< 0.001
Progression-free survival (PFS)	0.64	0.51–0.81	0.0002

Table 3. Survival outcomes based on *TP53* expression in COAD (TCGA data via TIMER2.0). Note: HR < 1 indicates reduced risk of event in high TP53 group.

Immune cell type	ρ (Spearman)	*p*-value	Association
Neutrophils	-0.9	< 0.01	Negative
B Cell Plasma	-0.87	< 0.01	Negative
M2 Macrophages	0.86	< 0.01	Positive

Table 4. Correlation between *TP53* expression and immune cell infiltration in COAD. Note: Correlations derived from TCGA-COAD data via TIMER2.0 and TISIDB.

Reactive oxygen species content

Estimating ROS in HT-29 cell lysate revealed that CFLE significantly increases ROS (148.7 pg/mL) compared to untreated control (130.4 pg/mL, $p = 0.0019$). CFLE + nanogold (141 pg/mL) elevate ROS non- significantly relative to control ($p = 1.0$). CFLE alone produces significantly higher ROS than CFLE + nanogold ($p = 0.0104$).

Bioinformatic analyses

Clinical correlations in COAD: TP53, immune Infiltration, and chemokine signaling (TCGA via TISIDB)

Survival analysis (TIMER2.0) Survival analysis via TIMER2.0 revealed that elevated *TP53* expression is significantly associated with better clinical outcomes in COAD patients. Patients with high *TP53* expression exhibited markedly improved overall survival (HR = 0.61, 95% CI: 0.48–0.78, $p = 0.0001$), disease-specific survival (HR = 0.59, 95% CI: 0.45–0.77, $p < 0.001$), and progression-free survival (HR = 0.64, 95% CI: 0.51–0.81, $p = 0.0002$) compared to those with low *TP53* expression (Table 3). These findings indicate that high *TP53* levels are a strong favorable prognostic factor in COAD.

TP53 expression correlation with immune cell infiltration Analysis of immune cell infiltration revealed significant associations between *TP53* expression and key components of the tumor immune microenvironment. As shown in Table 4, *TP53* expression exhibited strong negative correlations with neutrophil infiltration (ρ = -0.90, $p < 0.01$) and plasma B cells (ρ = -0.87, $p < 0.01$), while showing a positive correlation with M2 macrophages (ρ = 0.86, $p < 0.01$). This counterintuitive positive association with M2 macrophages may reflect tumor subtype heterogeneity or compensatory immune regulation in *TP53*-wild-type tumors.

TP53 regulates key chemokine networks involved in immune recruitment *TP53* expression was significantly and negatively correlated with multiple chemokines involved in neutrophil and myeloid cell recruitment (Fig. 7). As detailed in Table 5, strong negative correlations were observed for *CXCL1*, *CXCL2*, *CXCL3*, *CXCL5*, *CXCL6*, *CXCL8*, *CXCL11*, *CCL2*, *CCL7*, and *CCL20* (all $p < 0.001$, ρ ranging from − 0.65 to -0.74). These findings suggest that functional *TP53* suppresses pro-inflammatory chemokine signaling, potentially limiting neutrophil-driven tumor promotion.

In contrast, several chemokines and receptors showed no significant correlation with *TP53* expression (Table 6), including *CXCL12* (ρ = -0.03, $p = 0.62$), *CX3CL1* (ρ = 0.01, $p = 0.89$), *CCL1* (ρ = -0.12, $p = 0.08$), *CCL14* (ρ = -0.09, $p = 0.15$), *CCL19* (ρ = -0.07, $p = 0.25$), *CCL21* (ρ = -0.03, $p = 0.51$), *CCL28* (ρ = -0.04, $p = 0.53$), *XCL1* (ρ = -0.06, $p = 0.34$), *CCR7* (ρ = -0.04, $p = 0.41$), and *CCR9* (ρ = 0.02, $p = 0.67$) indicating that these pathways operate independently of *TP53* status and may be regulated by tissue-specific or alternative oncogenic mechanisms.

Immune phenotype stratification by TP53 status As summarized in Table 7 and illustrated in Fig. 7, tumors with *TP53* mutations exhibit a distinct immunosuppressive microenvironment characterized by high infiltration of M2 macrophages and neutrophils, suppressed B-cell recruitment, and increased T-cell exhaustion markers (e.g., PD-1, CTLA-4). In contrast, *TP53* wild-type tumors display more balanced immune activation, with enhanced adaptive immunity and reduced myeloid-derived suppression.

T-cell exhaustion in TP53-mutant tumors Table 8 notes increased T-cell exhaustion markers (PD-1, CTLA-4) in TP53-mutant tumors.

Discussion

Colon and rectal cancers are rare in developing countries but prevalent in developed ones, causing over 940,000 cases and nearly 500,000 deaths yearly. Diets high in animal protein, refined carbs, and fats, combined with low physical activity, are major risk factors. Hereditary factors account for less than 5% of cases. Increasing fruit and vegetable intake while reducing meat consumption, particularly processed meat, may lower risk[1].

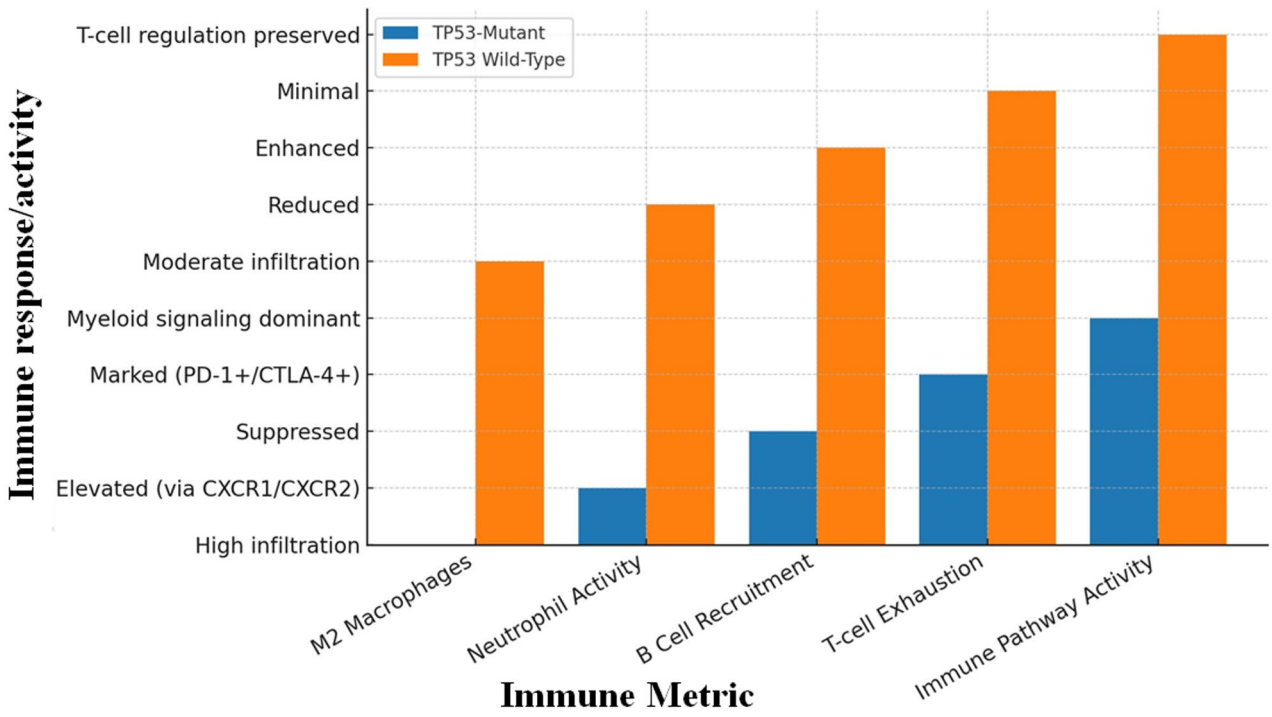

Fig. 7. Comparison of immune metrics between TP53-mutant and wild-Type COAD patients.

Chemokine	ρ (Spearman)	*p*-value	Primary function
CXCL8	-0.74	< 0.001	Neutrophil recruitment, angiogenesis
CXCL1	-0.72	< 0.001	Neutrophil chemotaxis (ELR + CXC)
CXCL6	-0.71	< 0.001	Neutrophil activation
CXCL2	-0.7	< 0.001	Neutrophil recruitment
CCL20	-0.69	< 0.001	Treg/Th17 cell recruitment
CXCL11	-0.69	< 0.001	T cell recruitment (inflammatory)
CXCL3	-0.68	< 0.001	Neutrophil chemoattractant
CCL2	-0.67	< 0.001	Monocyte/macrophage recruitment
CCL7	-0.66	< 0.001	Monocyte and dendritic cell chemoattraction
CXCL5	-0.65	< 0.001	Neutrophil recruitment

Table 5. Significant negative correlations between *TP53* expression and chemokines in COAD.

Plants have long been used as medicine, among humanity's earliest remedies, and remain important despite modern pharmaceutical advances. *Coleus forskohlii*, an edible plant used in Ayurvedic medicine, contains forskolin, a potent adenylate cyclase activator that raises cAMP levels and may affect cancer, eczema, rheumatism, obesity, blood pressure, and heart function. This study evaluated the biological activity of *C. forskohlii* extracts alone or combined with gold nanoparticles, specifically their effects on HT-29 colon cancer cells.

The emergence of a sharp absorption band in the visible region (~ 510–550 nm) is a hallmark of colloidal gold nanoparticle formation. This Surface Plasmon Resonance (SPR) arises from the collective oscillation of conduction electrons at the nanoparticle surface when interacting with light. Absence of SPR in extract alone where the extract shows no absorption beyond ~ 450 nm, confirming that the SPR band in the CFLE + nanogold is not due to plant pigments but results specifically from formed nanogold. The UV absorption of the extract alone below 400 nm corresponds to electron-rich biomolecules (e.g., phenolics, alkaloids, terpenes like forskolin), which act as reducing agents (converting $Au^{3+} \rightarrow Au^{0}$) and capping/stabilizing agents preventing aggregation[19]. In our work, FTIR study revealed that CFLE contains many active groups which helped CFLE to reduce and cap gold ions to synthesize stable nanogold. Confirmation of green synthesis as shown by the clear emergence of the SPR band provides rapid, non-destructive confirmation of successful green synthesis of nanogold using only plant extract, aligning with sustainable nanotechnology principles.

Chemokine/Receptor	ρ (Spearman)	*p*-value	Biological function
CXCL12	0.03	0.62	Stem cell homing, angiogenesis, metastasis
CX3CL1	0.01	0.89	Leukocyte adhesion
CCL19	0.07	0.25	CCR7 ligand; lymphoid homing
CCL1	-0.12	0.08	Lymphocyte recruitment
CXCL14	-0.09	0.15	Dendritic cell chemoattractant
CCL28	0.04	0.53	Mucosal immunity
CCL21	-0.03	0.51	Lymphoid tissue homing
XCL1	-0.06	0.34	Dendritic/NK cell recruitment
CCR7	-0.04	0.41	Lymphoid tissue trafficking
CCR9	0.02	0.67	Intestinal immunity
CX3CR1	—	0.18	Leukocyte adhesion

Table 6. Chemokines and receptors with non-significant correlation to *TP53* expression.

Immune metric	TP53-Mutant	TP53 Wild-type
M2 macrophages	High infiltration	Moderate infiltration
Neutrophil activity	Elevated (via CXCR1/CXCR2)	Reduced
B Cell recruitment	Suppressed	Enhanced
T-cell exhaustion	Marked (PD-1+/CTLA-4+)	Minimal
Immune pathway activity	Myeloid signaling dominant	T-cell regulation preserved

Table 7. Immune features by TP53 status in COAD. Note: TP53 status shapes the immune landscape, influencing response to immunotherapy.

XRD study of the created nanogold uncovered that the average nanogold size is about 58.90 nm. Many investigators could produce nanoparticles with different shapes using extracts of *Coleus forskohlii*[20,21]. The presence of characteristic fcc Au diffraction peaks unambiguously verify the successful bio-reduction of Au^{3+} (from $HAuCl_4$) to elemental gold (Au^0) by phytochemicals in the *Coleus forskohlii* extract. This XRD data demonstrates that plant-mediated synthesis (a green chemistry approach) can yield highly crystalline nanoparticles without the need for toxic chemical reductants (e.g., $NaBH_4$) or stabilizers. The absence of extra peaks (e.g., at ~ 30–35° that might indicate Au_2O_3 or other impurities) confirms phase-pure metallic gold, essential for applications in catalysis, sensing, and biomedicine. Crystalline, pure, and biocompatible AuNPs synthesized using *C. forskohlii* may leverage the plant's inherent bioactive compounds (e.g., forskolin) for enhanced therapeutic or synergistic effects in drug delivery or antimicrobial applications.

Natural products are renowned for their remarkable bioactive properties and consistent quality, making them invaluable in the development of new medicines. Cytotoxicity assays exhibit a broad range of sensitivity and can effectively identify numerous promising anticancer agents that selectively target and inhibit the biochemical pathways of various cancer cells[22]. The results of the current study clearly showed that treatment of the HT-29 cell line with the IC_{50} concentration of CFLE inhibited cancer cell growth, with activity persisting even when CFLE was diluted to 500 µg/mL. When the CFLE contained nanogold, the power of CFLE to inhibit cancer cell growth increased till the dilution 125 µg/mL. Nanogold has been extensively researched and is well-known in medicine. Malignant growth nanomedicines are now commonly used in cancer treatment due to their effectiveness and safety. The use of NPs in cancer therapy has greatly improved drug delivery compared to conventional methods[23].

The p53 protein is a vital tumor suppressor that manages cell cycle arrest, DNA repair, and apoptosis during cellular stress. Enhancing p53 levels is beneficial in cancer therapy, as it induces apoptosis in malignant cells. In our study, treatment HT-29 cells with *Coleus forskohlii* leaf extract (CFLE) alone lead to a significantly greater upregulation of p53 compared to control untreated cells. The measurable increase in p53 expression (likely due to bioactive compounds like forskolin, flavonoids, and phenolics), which can induce oxidative stress or DNA damage in cancer cells. The CFLE-containing nanogold formulation led to a measurable increase in p53 expression upregulation. This suggests that improved cellular uptake of phytochemicals due to nanoparticle-mediated delivery, synergistic bioactivity between gold nanoparticles and plant metabolites, enhanced pro-apoptotic signaling in HT-29 cells. The dramatic p53 response to CFLE + nanogold highlights the potential of green-synthesized nanophytocomposites as targeted anticancer agents. By boosting tumor suppressor pathways more effectively than the crude extract, this nano-formulation may offer a higher efficacy at lower doses, reduced off-target toxicity, a novel strategy for colorectal cancer therapy. Our data supports the growing paradigm that biogenic nanoparticles are not merely carriers but active contributors to biological effects, enhancing the pharmacological profile of traditional herbal medicines. The main p53 inhibitor, the E3 ubiquitin ligase MDM2, directs constitutive proteasomal degradation to keep p53 protein levels low in normal unstressed cells. The MDM4 (MDMX) protein is also a p53 inhibitor[24]. In our study, the addition of CFLE, in LC_{50} dose, increased

the expression of p53 protein levels in HT-29 cancer cell line over untreated control cells. When the nanogold was included in CFLE, the level of p53 little decreased less than CFLE alone.

Reactive oxygen species (ROS) are regulated by antioxidants and crucial for cell function. Disruption of redox balance can lead to diseases like cancer, where ROS levels are often high. While they play a role in carcinogenesis, they may also inhibit cancer due to differing antioxidant capacities in various cancer types[25]. The data indicate that *Coleus forskohlii* leaf extract (CFLE) significantly enhances intracellular reactive oxygen species (ROS) levels in HT-29 human colorectal adenocarcinoma cells compared to untreated controls. In contrast, the combination of CFLE with nanogold (CFLE + nanogold) resulted in a modest, non-significant increase in ROS, and produced significantly lower ROS than CFLE alone. These findings suggest that CFLE exerts a pro-oxidant effect, which is attenuated by nanogold conjugation. The significant elevation of ROS by CFLE aligns with the well-established anticancer mechanism of many phytochemicals that disrupt redox homeostasis in cancer cells. Elevated ROS can overwhelm antioxidant defenses (e.g., glutathione, superoxide dismutase), leading to mitochondrial dysfunction, DNA damage, and activation of intrinsic apoptotic pathways[26]. *Coleus forskohlii* contains bioactive diterpenes like forskolin, which has been shown to modulate cyclic AMP (cAMP) signaling and induce oxidative stress in cancer cells[27]. The lack of significant ROS elevation in the CFLE + nanogold group, coupled with significantly lower ROS than CFLE alone, suggests that gold nanoparticles may act as mild antioxidants or ROS scavengers in this system. Gold nanoparticles are known to exhibit catalase- or superoxide dismutase-mimetic activity, thereby neutralizing excess ROS[28]. This property may reduce the oxidative burst induced by CFLE, potentially altering its cytotoxic profile.

Phytomedicine utilizes different plant parts—seeds, berries, roots, leaves, barks, and blossoms—to prevent or treat diseases. Bioactive compounds in these plants offer promising avenues for new chemotherapies, especially with the emergence of multiresistant bacteria and the decreasing efficacy of current treatments[29]. The synergistic enhancement of antimicrobial efficacy in the CFLE + nanogold formulation likely arises from the dual action of phytochemicals and nanogold; phytochemicals (e.g., phenolics, forskolin derivatives) disrupt microbial membranes and interfere with metabolic enzymes, and gold nanoparticles increase membrane permeability via electrostatic interactions and may facilitate intracellular delivery of bioactive compounds. The loss of activity against *S. aureus* in the composite (zone decreased from 10.5 mm to 9.8 mm) suggests potential competitive binding between nanogold and *S. aureus*-targeting compounds, though the MIC remains in the same range (250–500 µg/mL), indicating no substantial loss of potency. Importantly, the emergence of anti-Gram-negative activity (especially against *E. coli*, from 0 to 8.2 mm) revealed that addition of nanogold to the extract overcomes the intrinsic resistance of Gram-negative bacteria, likely by disrupting the outer membrane via nanoparticle adhesion. This aligns with recent studies showing metal nanoparticles enhance penetration of plant extracts through lipopolysaccharide barriers[30,31].

The tumor microenvironment in colon cancer has a considerable impact on targeted cancer therapy. The tumor microenvironment is dynamic, containing a wide range of cell types including B cells, tumor-associated macrophages, regulatory T cells, neutrophils, and myeloid-derived suppressor cells, as well as extracellular factors that surround cancer cells and play functional and structural roles under physiological and pathological conditions[32]. In colon cancer, significant infiltration of B lymphocytes and plasma cells has a positive predictive impact on biomarker investigations related to the inflammatory tumor microenvironment[33]. Furthermore, metabolic alterations in M2 macrophages during colon cancer progression are associated with tumor prognosis[34]. Our bioinformatic analyses revealed that M2 Macrophages exhibited the strongest positive correlation with *TP53* expression. M2 macrophages are pro-tumoral, promoting tissue repair, angiogenesis, and immunosuppression. This suggests that tumors with high *TP53* expression (often mutant p53 protein accumulation) create a microenvironment favoring this immunosuppressive cell type. Positive correlation with M2 macrophages suggests that TP53 dysfunction (mutation or inactivation) is linked to tumor-promoting macrophage polarization. This may be mediated through indirect pathways involving CCL2, CCL7, and stromal factors like PDGFRB, which support immunosuppressive stroma. In addition, B Cell Plasma and Neutrophils showed a strong negative correlation. This indicates impaired humoral immunity and potentially altered innate immune responses in *TP53*-aberrant tumors. The chemokine CCL11 plays a crucial role in the control of colitis and related carcinogenesis, hence anti-CCL11 antibodies may be effective for inflammatory bowel syndrome therapy and cancer chemoprevention[35]. CL14 mRNA transcripts were highly expressed in the colon, particularly in Crohn's and ulcerative colitis patients[36]. Several studies have found that CCR1 and CCRL2 play a key role in organ colonization, and both chemokine receptors are potential therapy targets for early colorectal cancer[37]. Our bioinformatic analyses revealed that high TP53 expression is linked to significantly lower neutrophil infiltration. TP53 may suppress pro-neutrophil chemokines (e.g., CXCL1, CXCL8). Loss of plasma B cells in TP53-high tumors suggests impaired humoral immunity and B-cell recruitment. Despite TP53 being a tumor suppressor, its high expression correlates with reduced plasma B cell infiltration, indicating a complex role in adaptive immunity. This may reflect immune evasion mechanisms co-opted in certain tumor subtypes or feedback regulation in chronic inflammation. So, it suggests that tumors with high p53 expression have significantly fewer neutrophils and plasma B cells but are enriched for immunosuppressive M2 macrophages. TP53-mutant tumors are characterized by high M2 macrophages (immunosuppressive, pro-tumor), reduced plasma B cells (impaired humoral immunity) and increased neutrophils (via CXCR1/2 axis). TP53-wild-type tumors show more balanced immune infiltration and functional adaptive immunity. Results showed increased T-cell exhaustion markers (PD-1, CTLA-4) in TP53-mutant tumors. This suggests that TP53 status shapes adaptive immune dysfunction, possibly via altered chemokine networks (e.g., reduced CXCL11, involved in T-cell activation). Using gene expression data and immune deconvolution insights (consistent with CIBERSORT-ABS methodology), TP53 status in COAD is strongly associated with distinct immune infiltration patterns; loss of functional p53 drives a pro-inflammatory, neutrophil-dominated, and immunosuppressive TME, and p53 activity suppresses key chemokine modules involved in innate immune cell recruitment, highlighting its role as a regulator of tumor

Gene module	Associated immune cells	Relationship with TP53	Function in TME
CXCL1/2/3/5/6/8 – CXCR1/2	Neutrophils	Strong negative correlation	Drives neutrophil recruitment; upregulated in TP53-mutant COAD
CCL2/CCL7 – CCR2	Monocytes/M2 Macrophages	Negative correlation with TP53	Promotes M2 polarization and immunosuppression
CXCL11 – CXCR3	Activated T cells, NK cells	Negatively correlated ($\rho = -0.69$)	Loss in TP53-low tumors impairs anti-tumor immunity
PDGFRB	Cancer-associated fibroblasts (CAFs)	Negative correlation ($p = 0.003$)	Supports stromal remodeling and immune exclusion

Table 8. Gene modules and pathways involved.

immunogenicity. This gene module analysis provides a rationale for combining p53 status with immune profiling for prognosis and immunotherapy response prediction in COAD. In colon cancer, the epithelial-mesenchymal transition cascade is activated by the CCR3-ERK-JNK signaling axis[38]. This is not surprising given that our bioinformatic analyses revealed the clinical significance of p53 expression in COAD patients' survival as well as orchestrating the infiltration of immune cells within the tumor microenvironment, particularly B plasma cells and M2 macrophages, via CCL11 and CCL14 and their receptors CCR1, CCR2, and CRR3. Our survival analysis using TIMER2.0 demonstrates that high *TP53* expression is a robust predictor of improved survival in colon adenocarcinoma. This protective effect is closely linked to a favorable immune microenvironment characterized by reduced neutrophil recruitment, downregulation of pro-tumorigenic chemokines, and preservation of adaptive immune function. In contrast, *TP53* deficiency is associated with an immunosuppressive, neutrophil-rich tumor ecosystem that may contribute to aggressive disease and poor prognosis. These findings highlight *TP53* as both a prognostic biomarker and a central regulator of anti-tumor immunity in COAD.

Methods

Leaf extract from *Coleus forskohlii*

Plant samples were gathered from Al Soda, Aseer, Saudi Arabia in September 2022. The collection of the plant was done in accordance with the guideline set by Ethical Committee found at King Khalid University. The plant was kindly identified by the botanist Professor Ahmed Abas, biology department, faculty of science, King Khalid University, KSA, as *Coleus forskohlii* (Fig. 8) and a voucher specimen was deposited in biology department herbarium. Water extract was prepared from leaves of *Coleus forskohlii* (CFLE) was prepared exactly as done by Ibrahim et al.[39]. The dried materials were dissolved in water to get the stock solutions (1.3%), sterilized (syringe filter, 0.45 µm, Sigma-Aldrich) and stored at -35 °C.

Production of Nanogold and characterization

Nanogold (AuNPs) preparation/characterization were done the exactly as shown by Ibrahim et al.[40]. Briefly, 10 µL of 1 M chloroauric acid ($HAuCl_4$) was added to 10 mL CFLC (1 mg/mL) and mixed well. The pH of the mixture was raised stepwise by adding drops (in 10 µL volumes) of 1.5 M NaOH with mixing till the color of

Fig. 8. *Coleus forskohlii* plant collected from Al Soda Mountain, Aseer, KSA.

the mixtue changed. The change in color was evaluated spectrophotometrically at wavelengths 400–700 nm. X-ray diffraction (XRD) analysis was performed using a Shimadzu LabX XRD-6000 diffractometer operated at 40 kV and 35 mA. The diffractogram was recorded over a 2θ range of 20°–80° using CuKα radiation (wavelength λ = 1.540 Å). The average crystallite size (L) was estimated from the XRD pattern using the Debye–Scherrer equation:

$$D = \frac{k\lambda}{\beta cos\theta} \quad (1)$$

Where the shape factor k is constant, equals 0.9 (k is dimensionless), X-ray's beam wavelength λ in nm, β is known as the full width at half maximum (FWHM) of the peak in radian and the Braggs' diffraction angle is θ in degree[41].

Analysis of functional groups in CFLE

Bioactive groups found in CFLE were determined using Agilent Fourier transform infrared spectroscopy (FTIR, Cary 630 FTIR Spectrometer) at 4500 –500 cm^{-1} wavenumber.

Cell cytotoxicity assays

The American Type Culture Collection (ATCC) HT-29 colon cancer cell line was utilized this study. HT-29 cells were cultured and maintained utilizing the exact methods and reagents narrated by Ibrahim et al.[40]. Briefly, HT-29 human colon cancer cells were cultured in complete growth medium composed of Dulbecco's Modified Eagle Medium (DMEM, Hyclone) supplemented with 10% fetal bovine serum (FBS, Hyclone) and 1% penicillin–streptomycin solution (10,000 units/mL penicillin and 10,000 µg/mL streptomycin, Gibco). Cells were passaged upon reaching 70%–90% confluency. At confluence, the culture medium was aspirated, and the cell monolayer was washed twice with 2 mL of phosphate-buffered saline (PBS). Subsequently, 2 mL of trypsin (Gibco) was added to the flask and incubated for 3 min at 37 °C to detach the cells. Trypsinization was neutralized by adding 3 mL of complete medium. The resulting cell suspension was transferred to a 15 mL conical tube using a serological pipette and centrifuged at 350 × g for 5 min at 4 °C. Following centrifugation, the supernatant was discarded, and the cell pellet was resuspended in 1 mL of complete medium. For subculturing, 1 mL of this cell suspension was seeded into a new T-75 flask containing 9 mL of fresh complete medium. Cells were maintained in a humidified incubator at 37 °C with an atmosphere of 95% air and 5% CO_2 and were used within 10 consecutive passages for all experiments.

The study of CFLE and CFLE + nanogold cytotoxicity against the cancer cell line HT-29 was performed exactly as Ibrahim et al.[39] at a concentration gradient of 0–1000 µg/mL. Briefly, HT-29 colon cancer cells (5,000 cells per well) were seeded into 96-well plates (Corning) and incubated for 28 h in a CO_2 incubator to allow cell attachment and recovery. Following this, cells were treated with increasing concentrations of either CFLE or CFLE conjugated with nanogold (0, 0.49, 0.98, 1.95, 3.91, 7.81, 15.63, 31.25, 62.5, 125, 250, 500, and 1000 µg/mL). Each concentration was tested in triplicate wells, and the entire experiment was independently repeated 5 times. Control groups included untreated cells (cultured in complete medium only). Cell viability was assessed using the MTT assay and the percentage change in cell number (increase or decrease) relative to untreated controls was calculated according to the method outlined by Ibrahim et al.[39]. The half-maximal inhibitory concentration (IC_{50}), defined as the compound concentration that reduces cell viability by 50%, was determined by generating a dose–response curve. This curve was plotted using the mean absorbance values from the triplicate measurements across the tested concentration range, and IC_{50} values were derived via nonlinear regression analysis using GraphPad Prism 7.0 software.

Real time PCR for p53 gene expression quantification

Cancer cells (HT-29, 5×10^5 in 500 µL/well) were dispensed into 6-well culture plate wells and incubated in a CO_2-incubator for 20 h. After that, CFLE and CFLE + nanogold at IC_{50} concentration were separately added to the wells in triplicates and incubated for 48 h in a CO_2-incubator. Using the direction of an RNA extraction kit (RNeasy Mini Kit, Qiagen), total RNA was extracted from co-cultured HT-29 cells. Using a spectrophotometer (GENESY 10 UV Scanning, Thermo Scientific), total RNA was quantified at 260 nm, RNA purity was investigated at 280 nm, and integrity of RNA was speculated using 1.4% agarose gel (denaturing, Sigma-Aldrich) as shown by Adachi and Yu[42].

Using the reverse transcription kit (QuantiNova Reverse Transcription Kit), each extracted RNA sample (1 µg) was reverse transcribed into cDNA and then used to quantitatively detect p53 expressions using real-time polymerase chain reaction (PCR, Rotor-Gene Q 5plex Platform, QIAGEN).

Each reverse transcribed RNA (cDNA) was quantitatively amplified using QuantiNova Multiplex PCR Kits (QIAGEN) using the primer sets p53 F 5'- CCCCTCCTGGCCCCTGTCATCTTC-3', p53 R 5'-GCAGCGCCT CACAACCTCCGTCAT-3', β-actin F 5'-GTGACATCCACACCCAGAGG-3' and β-actin R 5'-ACAGGATGTC AAAACTGCCC-3' according to kit directions. The amplification protocol was reaction was 96 °C for 2 min as starting denaturing temperature (one cycle) followed by repeated cycles (36 cycles) composed of denaturing (92 °C), annealing (57 °C) and extension (72 °C), 18 s each[43]. Data were analyzed using built-in software.

Quantification of ROS in CFLE

Quantitative determination of reactive oxygen species (ROS) (Novatein Biosciences, USA) present in CFLE was done according to Ibrahim et al.[39] using EIAab ROS eia kit (Wuhan EIAab Science Co., Ltd.). The test was done following the manufacturer's instructions and the end products were read at 450 nm using BIOLINE ELISA reader (Bioline Diagnostics LLP).

Testing of antimicrobial power

The antimicrobial potentials of *Calotropis procera* leaf extract (CFLE), CFLE containing green-synthesized gold nanoparticles (CFLE + nanogold), and the standard antibiotic ciprofloxacin (5 µg) was evaluated using the agar well diffusion method and the minimum inhibitory concentration (MIC) against four bacterial strains namely *Escherichia coli* (Gram-negative), *Pseudomonas aeruginosa* (Gram-negative), *Bacillus subtilis* (Gram-positive), and *Staphylococcus aureus* (Gram-positive) as described by Ghramh et al.[44] and Szenci et al.[45] respectively. For the agar well diffusion method, all bacterial cultures were adjusted to a 0.5 McFarland standard ($\sim 1.5 \times 10^8$ CFU/mL) and uniformly spread onto Mueller-Hinton agar plates. Sterile 6-mm diameter wells were punched into the agar and loaded with 100 µL of CFLE (1 mg/mL), CFLE + nanogold (1 mg/mL), and Ciprofloxacin (50 µg/mL). Plates were incubated at 37 °C for 24 h, and the diameter of the inhibition zones (in millimeters), including the well diameter, was measured using a digital caliper in triplicate across 5 independent experiments.

For the MIC method, overnight cultures of each bacterial strain were adjusted to a 0.5 McFarland standard ($\sim 1 \times 10^8$ CFU/mL) and further diluted in Mueller–Hinton broth (MHB) to yield a final inoculum of $\sim 5 \times 10^5$ CFU/mL. Test compounds (CFLE and CFLE + nanogold) were serially diluted two-fold in MHB across a concentration range of 7.81–1000 µg/mL in 96-well microtiter plates. Ciprofloxacin served as a positive control. Plates were incubated aerobically at 37 °C for 20 h. The MIC was defined as the lowest concentration of the test agent that completely inhibited visible bacterial growth. All assays were performed in triplicate, and sterility and growth controls were included in each run.

Bioinformatic analyses

This analysis integrates in vitro results from HT-29 colon cancer cells treated with *Coleus forskohlii* leaf extract (CFLE) and CFLE conjugated with gold nanoparticles (CFLE + nanogold), with clinical genomic data from Colon Adenocarcinoma (COAD) patients via the Tumor–Immune System Interaction Database (TISIDB), which leverages The Cancer Genome Atlas (TCGA). The goal is to evaluate antiproliferative effects of CFLE and CFLE + nanogold, modulation of p53 gene expression in vitro, and correlations between TP53 (p53) expression and chemokines/immune infiltration in COAD patients.

TISIDB/TCGA analysis: p53 expression and immune microenvironment in COAD patients

To contextualize the experimental findings within human patient data, we analyzed The Cancer Genome Atlas (TCGA) data for Colon Adenocarcinoma (COAD) via the TISIDB portal. This reveals a complex relationship between p53 (TP53) expression and the tumor immune landscape.

TP53 expression and chemokine/receptor correlations

Using TISIDB, we performed multidimensional profiling to evaluate chemokine and receptor associations with *TP53* expression in COAD.

Survival analysis (TIMER2.0)

To assess the prognostic importance of TP53 expression in colon adenocarcinoma (COAD), a survival analysis was conducted utilizing the Tumor Immune Estimation Resource (TIMER2.0; [http://timer.cistrome.org/]), which is an integrated platform that harnesses transcriptomic and clinical data sourced from The Cancer Genome Atlas (TCGA). The analysis focused on overall survival (OS), disease-specific survival (DSS), and progression-free survival (PFS) among COAD patients, stratified according to TP53 mRNA expression into high and low expression groups, with the division determined by the median expression value for the cohort. Kaplan-Meier survival curves were constructed for each survival measure, and the statistical significance of the results was evaluated through the log-rank test. Hazard ratios (HR) with 95% confidence intervals (CI) were computed to define the relationship between TP53 expression and patient outcomes. A p-value of less than 0.05 was deemed statistically significant. Furthermore, to elucidate the role of TP53 within the tumor immune microenvironment, we examined the correlations between TP53 expression and the infiltration of immune cells (including B cells, M2 macrophages, and neutrophils), chemokine networks, and immune checkpoint pathways, employing data derived from TIMER2.0 and TISIDB. Spearman's rank correlation coefficients (ρ) were calculated to determine the strength and directionality of these associations. The infiltration levels of immune cells were estimated using deconvolution algorithms (such as TIMER and CIBERSORT), with only those correlations achieving $p < 0.01$ being classified as significant. Additionally, chemokines and receptors that displayed non-significant associations ($p > 0.05$) were recorded to identify immune pathways independent of TP53[46].

Statistical analysis

All experimental data were analyzed using appropriate statistical methods. Regarding antimicrobial activity, data are expressed as mean ± standard deviation (SD), $n = 5$. One-way analysis of variance (ANOVA) followed by Tukey's post hoc test was used to determine statistically significant differences between treatment groups. Our results were statistically significant at p-value ≤ 0.05. For cytotoxicity and p53 level experiments, a paired-samples t-test was performed using GraphPad Prism 7 (GraphPad Software, Inc., USA), and results were considered statistically significant at $p \leq 0.05$. Clinical and genomic data were integrated using R-based bioinformatics platforms (TIMER2.0 and TISIDB).

Conclusion

This study presents a novel approach by demonstrating, for the first time, that *Coleus forskohlii* leaf extract (CFLE), derived from an edible, traditionally used medicinal plant, can not only function as a green synthesis agent to produce stable nanogold particles (average diameter: 58.90 nm) but also exhibit potent anti-colon

cancer activity, both alone and in combination with the biosynthesized nanogold, against the HT-29 human colon adenocarcinoma cell line.

Furthermore, leveraging the TIMER2.0 platform, we uncover a previously underappreciated immunological dimension of TP53 in colorectal cancer: high TP53 expression strongly correlates with improved patient survival, a favorable immune microenvironment characterized by reduced neutrophil infiltration, lower levels of pro-tumorigenic chemokines, and preserved adaptive immunity. In stark contrast, TP53 deficiency fosters an immunosuppressive, neutrophil-rich tumor milieu linked to aggressive disease and poor prognosis.

Together, these findings highlight the dual novelty of our work; the innovative use of CFLE as both a therapeutic agent and a nanobiotechnological tool against colon cancer, and the elucidation of TP53's critical role as a regulator of anti-tumor immunity, offering new avenues for biomarker-driven and immune-modulating strategies in colorectal cancer management.

Data availability

All data and materials are available in the manuscript.

Received: 2 September 2025; Accepted: 9 December 2025
Published online: 19 January 2026

References

1. World Health Organization. Global cancer rates could increase by 50% to 15 million by 2020 (2020). https://www.who.int/news/item/03-04-2003-global-cancer-rates-could-increase-by-50-to-15-million-by-2020.
2. Aune, D. et al. Dietary fibre, whole grains, and risk of colorectal cancer: systematic review and dose-response meta-analysis of prospective studies. *BMJ* **343**, 1082 (2011).
3. Bradbury, K. E., Appleby, P. N. & Key, T. J. Fruit, vegetable, and fiber intake in relation to cancer risk: findings from the European prospective investigation into cancer and nutrition (EPIC). *Am. J. Clin. Nutr.* **100**, 394S–398S (2014).
4. Dzobo, K. The role of natural products as sources of therapeutic agents for innovative drug discovery. *Compr. Pharmacol.* **408**, 253. https://doi.org/10.1016/B978-0-12-820472-6.00041-4 (2022).
5. Lukhoba, C. W., Simmonds, M. S. J. & Paton, A. J. Plectranthus: a review of ethnobotanical uses. *J. Ethnopharmacol.* **103**, 1–24 (2006).
6. Maheswari, R. U., Selvamurugan, C., Jayabarath, J. & Prabha, A. L. Hairy root culture of an important medicinal plant: coleus forskohliI.. *Int. J. Agric. Sci.* **3**, 82–89 (2011).
7. Alasbahi, R. H. & Melzig, M. F. Plectranthus barbatus: a review of phytochemistry, ethnobotanical uses and Pharmacology part 2. *Planta Med.* **76**, 753–765 (2010).
8. Aiyelaagbe, O. O. & Osamudiamen, P. M. Phytochemical screening for active compounds in mangifera indica leaves from Ibadan, Oyo state. *Plant. Sci. Res.* **2**, 11–13 (2009).
9. Ammon, H. P. T. & Muller, A. B. Forskolin from an ayurvedic remedy to a modern agent. *Planta Med.* **6**, 473–477 (1985).
10. Sapio, L. et al. The natural cAMP elevating compound forskolin in cancer therapy: is it time? *J. Cell. Physiol.* **232**, 922–927 (2017).
11. Shivaprasad, H. N. et al. Ethnopharmacological and phytomedical knowledge of coleus forskohlii: an approach towards its safety and therapeutic value. *Orient. Pharm. Exp. Med.* **14**, 301–312 (2014).
12. Rout, O. P., Acharya, R., Mishra, S. K. & Sahoo, R. Pathorchur (Coleus aromaticus): a review of the medicinal evidence for its phytochemistry and Pharmacology properties. *Int. J. Appl. Biol. Pharm. Technol.* **3**, 348–355 (2012).
13. Loftus, H., Astell, K., Mathai, M. & Nutrients, X. S. & U. Coleus forskohlii extract supplementation in conjunction with a hypocaloric diet reduces the risk factors of metabolic syndrome in overweight and obese. *Nutrients* **7**, 9508–9522 (2015).
14. Tung, Y. C. et al. Coleus forskohlii and garcinia indica extracts attenuated lipid accumulation by regulating energy metabolism and modulating gut microbiota in obese mice. *Food Res. Int.* **142**, 236 (2021).
15. Suzuki, S. et al. Coleus forskohlii extract attenuated the beneficial effect of Diet-Treatment on NASH in mouse model. *J. Nutr. Sci. Vitaminol (Tokyo).* **66**, 191–199 (2020).
16. Boomi, P. et al. Biological synergy of greener gold nanoparticles by using coleus aromaticus leaf extract. *Mater. Sci. Eng. C Mater. Biol. Appl.* **99**, 202–210 (2019).
17. Sathyavathi, R., Krishna, M. B., Rao, S. V. & Saritha, R. Biosynthesis of silver nanoparticles using coriandrum sativum leaf extract and their application in nonlinear optics. *Adv. Sci. Lett.* **3**, 138–143 (2010).
18. Shameli, K., Ahmad, M., Bin, Yunus, W. Z. W., Ibrahim, N. A. & Darroudi, M. Synthesis and characterization of silver/talc nanocomposites using the wet chemical reduction method. *Int. J. Nanomed.* **5**, 743 (2010).
19. Pavitra Dasari, P., Baburao, N., Chekuri, S. & Rani, A. R. Evaluation of phytochemical screening of coleus forskohlii L. leaf extract. *J. Phytopharm.* **7**, 437–439 (2018).
20. Dhayalan, M. et al. Biogenic synthesis, characterization of gold and silver nanoparticles from coleus forskohlii and their clinical importance. *J. Photochem. Photobiol. B Biol.* **183**, 251–257 (2018).
21. Naraginti, S. & Sivakumar, A. Eco-friendly synthesis of silver and gold nanoparticles with enhanced bactericidal activity and study of silver catalyzed reduction of 4-nitrophenol. *Spectrochim Acta Part. Mol. Biomol. Spectrosc.* **128**, 357–362 (2014).
22. Kamaleeswari, M., Deeptha, K., Sengottuvelan, M. & Nalini, N. Effect of dietary Caraway (Carum carvi L.) on aberrant crypt foci development, fecal steroids, and intestinal alkaline phosphatase activities in 1,2-dimethylhydrazine-induced colon carcinogenesis. *Toxicol. Appl. Pharmacol.* **214**, 290–296 (2006).
23. Bharadwaj, K. K. et al. Green synthesis of gold nanoparticles using plant extracts as beneficial prospect for cancer theranostics. *Molecules* **26**, 236 (2021).
24. Hassin, O. & Oren, M. Drugging p53 in cancer: one protein, many targets. *Nat. Rev. Drug Discov.* **22**, 127–144 (2022).
25. Yang, Y., Karakhanova, S., Werner, J. & Bazhin, A. Reactive oxygen species in cancer biology and anticancer therapy. *Curr. Med. Chem.* **20**, 3677–3692 (2013).
26. Zhao, Y. et al. Cancer metabolism: the role of ROS in DNA damage and induction of apoptosis in cancer cells. *Metabolites* **13**, 253 (2023).
27. Roshni, P. T. & Rekha, P. D. Biotechnological interventions for the production of forskolin, an active compound from the medicinal plant, coleus forskohlii. *Physiol. Mol. Biol. Plants* **30**, 213 (2024).
28. Pan, Y. et al. Size-dependent cytotoxicity of gold nanoparticles. *Small* **3**, 1941–1949 (2007).
29. Hemeg, H. A. et al. Antimicrobial effect of different herbal plant extracts against different microbial population. *Saudi J. Biol. Sci.* **27**, 3221 (2020).
30. Sa'ed, M. M., Ayivi, R. D., Wei, J. & Obare, S. O. Gold nanoparticles antibacterial activity: does the surface matter? *Colloid Interface Sci. Commun.* **62**, 100804 (2024).
31. Parvin, N., Joo, S. W. & Mandal, T. K. Nanomaterial-Based strategies to combat antibiotic resistance: mechanisms and applications. *Antibiot. 2025.* **14**, 207 (2025).

32. Gallo, G., Vescio, G., De Paola, G. & Sammarco, G. Therapeutic targets and tumor microenvironment in colorectal cancer. *J. Clin. Med.* **10**, 1452 (2021).
33. Berntsson, J., Nodin, B., Eberhard, J., Micke, P. & Jirström, K. Prognostic impact of tumour-infiltrating B cells and plasma cells in colorectal cancer. *Int. J. Cancer*. **139**, 1129–1139 (2016).
34. Huang, F. et al. M2 macrophage classification of colorectal cancer reveals intrinsic connections with metabolism reprogramming and clinical characteristics. *Pharmgenomics Pers. Med.* **17**, 383–399 (2024).
35. Polosukhina, D. et al. CCL11 exacerbates colitis and inflammation-associated colon tumorigenesis. *Oncogene* **40**, 6540–6546 (2021).
36. Kotarsky, K. et al. A novel role for constitutively expressed epithelial-derived chemokines as antibacterial peptides in the intestinal mucosa. *Mucosal Immunol.* **3**, 40–48 (2010).
37. Akram, I. G., Georges, R., Hielscher, T., Adwan, H. & Berger, M. R. The chemokines CCR1 and CCRL2 have a role in colorectal cancer liver metastasis. *Tumour Biol.* **37**, 2461–2471 (2016).
38. Lee, Y. S. et al. Crosstalk between CCL7 and CCR3 promotes metastasis of colon cancer cells via ERK-JNK signaling pathways. *Oncotarget* **7**, 36842 (2016).
39. Ibrahim, E. H. et al. Potency of Moringa Oleifera leaf extract and silver nanoparticles against immune, microbial and HT-29 colon cancer cells growth modulation. *Pak. J. Pharm. Sci.* **35**, 827–834 (2022).
40. Ibrahim, E. H. et al. Origanum Majorana harvested from Al-Soda, Saudi Arabia promotes mitotic arrest and apoptosis in colon cancer cells. *J. King Saud Univ. - Sci.* **34**, 101878 (2022).
41. Dubey, S. P., Lahtinen, M. & Sillanpää, M. Tansy fruit mediated greener synthesis of silver and gold nanoparticles. *Process. Biochem.* **45**, 1065–1071 (2010).
42. Adachi, H. & Yu, Y. T. Purification of radiolabeled RNA products using denaturing gel electrophoresis. *Curr. Protoc. Mol. Biol.* **105**, 20 (2013).
43. Ibrahim, E. H. et al. Lepidium sativum and its biogenic silver nanoparticles activate immune cells and induce apoptosis and cell cycle arrest in HT-29 colon cancer cells. *Biomater. Tissue Eng.* **11**, 195–209 (2021).
44. Ghramh, H. A., Ibrahim, E. H. & Ahmad, Z. Antimicrobial, Immunomodulatory and cytotoxic activities of green synthesized nanoparticles from acacia honey and Calotropis procera. *Saudi J. Biol. Sci.* **28**, 3367–3373 (2021).
45. Szenci, O. et al. Determination of minimum inhibitory concentrations of selected antibiotics against Trueperella pyogenes originated from bovine clinical endometritis. *Pathog 2025.* **14**, 405 (2025).
46. Ru, B. et al. TISIDB: an integrated repository portal for tumor-immune system interactions. *Bioinformatics* **35**, 4200–4202 (2019).

Acknowledgements

The authors extend their appreciation to the Deanship of Research and Graduate Studies at King Khalid University for funding this work through Large Research Project under grant number RGP.2/330/45.

Author contributions

All authors contributed equally in this work.

Funding

This work was funded by Deanship of Research and Graduate Studies at King Khalid University, grant number RGP.2/330/45.

Competing interests

The authors declare no competing interests.

Additional information

Correspondence and requests for materials should be addressed to E.H.I.